Atmos. Chem. Phys. Discuss., https://doi.org/10.5194/acp-2018-49
Manuscript under review for journal Atmos. Chem. Phys.
Discussion started: 29 January 2018

Atmospheric Chemistry and Physics Discussions

Light absorption of brown carbon in eastern China based on 3-year multi-wavelength aerosol optical property observations at the SORPES station and an improved Absorption Ångstrom exponent segregation method

Jiaping Wang[1,2,3], Wei Nie[1,2], Yafang Cheng[3,4], Yicheng Shen[1,2], Xuguang Chi[1,2], Jiandong Wang[4], Xin Huang[1,2], Yuning Xie[1,2], Peng Sun[1,2], Zheng Xu[1,2], Ximeng Qi[1,2], Hang Su[3,4,2], and Aijun Ding[1,2*]

[1]Joint International Research Laboratory of Atmospheric and Earth System Sciences, School of Atmospheric Sciences, Nanjing University, Nanjing, 210023, China
[2]Jiangsu Provincial Collaborative Innovation Center for Climate Change, Nanjing, 210023, China
[3]Max-Plank Institute for Chemistry, Germany
[4]Research Institute for Climate and Environment, Jinan University, Guangzhou
*Correspondence to: Aijun Ding (dingaj@nju.edu.cn)

Abstract. Brown carbon (BrC), a certain group of organic carbon (OC) with strong absorption from the visible to ultraviolet (UV) wavelengths, makes considerable contribution to light absorption on both global and regional scales. High concentration and proportion of OC has been reported in China, but studies of BrC absorption based on long-term observations are rather limited in this region. In this study, we reported 3-year results of light absorption of BrC based on continuous measurement at the Station for Observation Regional Processes of the Earth System (SORPES) in the Yangtze River Delta, China combined with Mie-theory calculation. Light absorption of BrC was obtained using an improved Absorption Ångstrom exponent (AAE) segregation method to calculate AAE of 'pure' and non-absorbing coated black carbon (BC) at each time step based on Mie-theory simulation and measurement of multi-wavelength aerosol light absorption. By using this improved method, the variation of AAE over time is taken into consideration, making it applicable for long-term analysis. The yearly average light absorption of BrC (b_{abs_BrC}) at 370 nm was 4.3 Mm^{-1} at the SORPES station. The contribution of BrC to total aerosol absorption (P_{BrC}) at 370 nm ranged from 6% to 18% (10^{th} and 90^{th} percentiles, respectively), and reached up to ~28% in biomass burning-dominant season and winter.

Atmos. Chem. Phys. Discuss., https://doi.org/10.5194/acp-2018-49
Manuscript under review for journal Atmos. Chem. Phys.
Discussion started: 29 January 2018

Both b_{abs_BrC} and P_{BrC} exhibited clear seasonal cycles with two peaks in later spring/early summer (May-June, b_{abs_BrC}~4 Mm^{-1}, P_{BrC}~11%) and winter (December, b_{abs_BrC}~12 Mm^{-1}, P_{BrC}~17%), respectively. Lagrangian modeling and chemical signature observed at the site suggested that open biomass burning and residential emissions were the dominate sources influencing BrC in the two seasons.

Atmos. Chem. Phys. Discuss., https://doi.org/10.5194/acp-2018-49
Manuscript under review for journal Atmos. Chem. Phys.
Discussion started: 29 January 2018

1 Introduction

Atmospheric aerosols not only pose adverse impacts on human health, but also alter earth's radiation balance through their strong light scattering and absorption, substantially influencing regional and even global climate change (IPCC, 2013;Dockery et al., 1993;Wang et al., 2017b). Light absorption of aerosols strongly influence the magnitude and sign of radiative transfer. Black carbon (BC) and dust have been considered as two dominant contributors to aerosol absorption extinction. However, a certain type of organic aerosol defined as brown carbon (BrC) was revealed to be of strong light-absorbing efficiency (Bahadur et al., 2012;Pöschl, 2003), which can pose perturbations on radiation transfer similar to BC. This implies that aerosol cooling effect could be overestimated by ignoring the light absorption from BrC. Its strong light absorption in UV range can also affect atmospheric oxidizing capacity by restraining the photolysis rates for photochemically active gases (Laskin et al., 2015). It has been reported that the radiative forcing by BrC globally is about one fourth of that by BC (Feng et al., 2013), while regional radiative forcing by BrC in areas with intensive combustion activities (e.g. South and East Asia, South America, and Africa) can be much higher than global average, indicating the substantial contribution by BrC to aerosol light absorption in these regions and thereby significantly influence regional climate change. Therefore, investigation on BrC contribution to light absorption is of great importance to reduce the uncertainties of aerosol-radiation interaction (ARI) estimation.

BrC is defined as the organic carbon which can absorb solar radiation efficiently in near-UV (300 ~ 400 nm) to visible ranges (Pöschl, 2003). It is a group of species with specific physical property but difficult to characterize detailed chemical components. BrC can be produced not only from primary emissions relating to biomass burning and fuel combustion, but also from secondary organic aerosol (SOA) formation through oxidation of volatile organic compounds (VOCs) (Andreae and Gelencsér, 2006;Saleh et al., 2014;Chen and Bond, 2010;Lack et al., 2012;Laskin et al., 2015). Some studies reported that vehicle and marine emissions may also be the sources of BrC (Stone et al., 2009;Cavalli et al., 2004). The complication of the emitted mixtures containing BC, BrC, non-absorbing OA, and inorganic materials in different proportions makes it difficult to perform source attribution and to estimate its emission factor (EF).

Atmos. Chem. Phys. Discuss., https://doi.org/10.5194/acp-2018-49
Manuscript under review for journal Atmos. Chem. Phys.
Discussion started: 29 January 2018

Light absorption of BrC is usually estimated based on its strong wavelength dependence with higher absorption from visible to UV range. The wavelength dependence of the aerosol absorption coefficient (b_{abs}) is normally represented by absorption Ångstrom exponent (AAE) and its relationship with b_{abs} is $b_{abs}(\lambda) \propto \lambda^{-AAE}$ (Moosmüller et al., 2011;Sun et al., 2007). Based on the difference of wavelength dependence for BC and BrC, light absorption of BrC can be segregated from multi-wavelength optical measurements (e.g. aethalometer), which is called AAE method. Usually, AAE of BC (AAE_{BC}) was set to be 1.0 based on the properties of bulk BC by many previous studies, assuming the unity of AAE_{BC} between any two wavelengths within UV to near inferred (IR) range (Shen et al., 2017b;Olson et al., 2015;Lack and Langridge, 2013). However, the large uncertainty was mentioned by Lack and Langridge (2013) using this assumption and also this method can only be used when the proportion of BrC is high. Moreover, it is noticed lately that AAE of BC is not always 1.0, instead, it can be affected by particle size and mixing state (Lack and Cappa, 2010).

China, the largest country in East Asia with tremendous fossil fuel and biofuel consumption and extensive agricultural burning, is of great concern in terms of its large contribution of carbonaceous aerosols including light absorbing carbon (BC, BrC) (Ding et al., 2016a). BC issue has been noticed in recent years in China, including its temporal variations, emission sources, climate effect (Cao et al., 2006;Cao et al., 2009;Yang et al., 2009;Wang et al., 2017a;Huang et al., 2014) as well as its 'dome effect' in modifying the boundary layer and enhancing haze pollution in megacities (Ding et al., 2016b). Organic matter(OM) is a large contributor to $PM_{2.5}$ in China (15%-51% of $PM_{2.5}$, Wang et al., 2017c), especially in the Yangtze River Delta (YRD) region, which is one of the most densely populated city cluster in eastern China and also an important agricultural center with crops planted in both cold and warm seasons (Ding et al., 2013c). In YRD region, OM fraction is 20%-40% of $PM_{2.5}$ mass (Wang et al., 2017c;Wang et al., 2017b) due to the influence by complicated combustion sources, therefore, BrC is a highly possible to be the contributor to aerosol light absorption in this region. However, studies concerning BrC in China, especially YRD region, are still limited up to now. Yuan et al. (2016) reported light absorption contributions of BrC in the Pearl River Delta (PRD) region to be 6.3% to 12.1% at

Atmos. Chem. Phys. Discuss., https://doi.org/10.5194/acp-2018-49
Manuscript under review for journal Atmos. Chem. Phys.
Discussion started: 29 January 2018

405nm in autumn and winter campaigns by using the AAE method. Shen et al. (2017b) conducted light absorption measurement in Xi'an in summer and winter, and reported the average $b_{abs\_BrC\_370}$ of 6.4 Mm^{-1} and 43.0 Mm^{-1} in the two seasons, respectively, based on AAE method. Yang et al. (2009) derived mass absorption efficiency (MAE) at 370 nm and $AAE_{470\text{-}660}$ of BrC which was 2.2 $m^2\ g^{-1}$ and 3.5, respectively during campaign in March 2015 at Xianghe in North China. It is noticed that long-term investigation of BrC light absorption in YRD region has not been reported yet.

This study intends to provide a comprehensive analysis on light-absorbing characteristics of BrC and its influencing factors based on field measurement of multi-wavelength aerosol light absorption at the SORPES station in Nanjing in the western YRD region and an improved AAE segregation method based on Mie-theory simulation. The contribution of BrC to light absorption is estimated based on a 3-year observation and the potential sources of BrC in typical seasons are discussed.

2 Measurements of optical properties and relevant species

Field observation was conducted at the Station for Observing Regional Processes of the Earth system (SORPES), located in the Xianlin campus of Nanjing University on top of a small hill (118°57′10″E, 32°07′14″ N; 40 m a.s.l.) (Shen et al., 2017a;Ding et al., 2013c;Ding et al., 2016a). The SORPES station is a research and experiment platform in western YRD, which is under influence of intensive human activities (Ding et al., 2016a). Since this observation site is about 20 km east of the city center and it is generally upwind from city center. Also, under influence of East Asian monsoon, this site is generally downwind of densely populated city cluster including the megacity Shanghai. Therefore, this station can be considered as a regional background station in the western YRD region and is an ideal site to study the impact of multiple anthropogenic emission on regional air quality in eastern China (Ding et al., 2016a;Ding et al., 2013a).

Optical properties were measured from 1 June 2013 to 31 May 2016. Aerosol light absorption measurement was conducted using a multi-wavelength Aethalometer (Model AE-31, Magee Scientific Company Berkeley, California, USA), which performs continuous measurements at seven wavelengths,

Atmos. Chem. Phys. Discuss., https://doi.org/10.5194/acp-2018-49
Manuscript under review for journal Atmos. Chem. Phys.
Discussion started: 29 January 2018

i.e., 370 nm in ultraviolet (UV) wavelength range (UV), 470 nm, 520 nm, 590 nm, 660 nm, 880 nm in visible (VIS) wavelength range, and 950 nm in infrared (IR) wavelength range. The time resolution is 5 min. Sample air was obtained through a stainless-steel inlet with a $PM_{2.5}$ cut cyclone (Very Sharp Cut Cyclone, VSCC, BGI Inc.), protected with a rain cap. The sample flowrate of the aethalometer was set to 5.0 liter per minute (LPM). In this study, the measurements at 370 nm, 520 nm and 880 nm were used for further analysis. The wavelength of 370 nm was used because studies have found that BrC shows strong light absorption near UV wavelength range (Andreae and Gelencsér, 2006;Hansen and Schnell, 2005). Measurement data at the wavelength of 880 nm was chosen because light absorption at this wavelength normally represents the BC absorption (Virkkula et al., 2015). The wavelength of 520 nm was used for the following calculations. b_{abs} at each wavelength was calculated using the method presented by Collaud Coen et al. (2010) to correct the systematic errors of filter-based absorption measurements,. Detailed description of the correction can be found in Shen et al. (2017a). Absorption coefficients were presented under Standard Temperature and Pressure (STP, i.e. 273.15 K, 1013 hPa).

OC and EC measurements were conducted using a Semi-Continuous Carbon Aerosol Analyzer (Sunset, Model-4, Sunset Laboratory Inc.) using RTQuartz sample analysis protocol, which is the short version of the NIOSH 5040. The ambient air was obtained through the $PM_{2.5}$ cut cyclone and the inlet tubing was protected by a rain cap. The sample flow rate was set to 8.0 LPM. A quartz filter was mounted in the quartz oven and samples were collected for the specified time. After the sample was collected, the system closed off the sample port, purging the analytical flowpath with helium and performing the thermal/optical analysis. The thermally removed carbon components were converted to CO_2, which was subsequently measured by non-dispersive infrared (NDIR). Correction for the pyrolytically generated carbon was based on filter absorbance measurements using a laser absorbance technique. Data collection was from 1 June 2014 to 31 May 31 2015. To convert the ratio of OC/EC to V_{OM}/V_{EC}, OM/OC was set to 1.6 according to the study from Aiken et al. (2008). V_{OM}/V_{EC} was then computed as $\frac{V_{OM}}{V_{EC}} = (\frac{OM}{EC})/(\frac{\rho_{OM}}{\rho_{EC}})$, where ρ_{OM} and ρ_{EC} represent the densities of OM and EC which was set to 1.4 and 1.8 (in g cm^{-3}), respectively (Pitchford et al., 2007). In present study, water-soluble ions (K^+,

Atmos. Chem. Phys. Discuss., https://doi.org/10.5194/acp-2018-49
Manuscript under review for journal Atmos. Chem. Phys.
Discussion started: 29 January 2018

Cl^-) were measured by the Monitor for Aerosols and Gases in Air (MARGA, Metrohm Co.), $PM_{2.5}$ and meteorological data were used for further supporting discussions. More detailed descriptions of these measurements can be found in Ding et al. (2013b, c; 2016a).

3 Estimation of BrC light absorption with an improved AAE method

It has been proved that BrC shows strong light absorbance in UV-visible wavelength range. To quantify the light absorption of BrC based on optical measurement results, the following method is proposed. Light absorption of BrC is calculated as the result of b_{abs} minus b_{abs_BC} at 370 nm. Here $b_{abs\_BC\_370}$ is defined as the absorption coefficient of pure BC or BC with non-absorbing coating at 370 nm, and b_{abs_BrC} is obtained from the following equation:

$$b_{abs\_BC\_370} = b_{abs\_880} \times (880/520)^{AAE_{BC520-880}} \times (520/370)^{AAE_{BC370-520}} \quad Eq.\ 1$$

$$b_{abs\_BrC} = b_{abs\_370} - b_{abs\_BC\_370} \quad Eq.\ 2$$

where b_{abs_370} and b_{abs_880} represents the absorption coefficients at 370 nm and 880 nm, respectively, which is calculated from the light absorption measurement data. $AAE_{BC520\text{-}880}$ and $AAE_{BC370\text{-}520}$ stands for the AAE of pure BC and BC with non-absorbing coating at long and short wavelength ranges. AAE at two wavelengths is calculated as the following equation:

$$AAE_{\lambda 1-\lambda 2} = -\frac{\ln(b_{abs_{\lambda 1}}) - \ln(b_{abs_{\lambda 2}})}{\ln(\lambda 1) - \ln(\lambda 2)} \quad Eq.\ 3$$

Previous studies have reported that the AAE of pure BC without coating or with non-absorbing coating is close to 1.0, and the AAE value of 1.0 was adopted for BC by many researches (Shen et al., 2017b;Olson et al., 2015;Lack and Langridge, 2013). However, there have been evidences showing that AAE of pure BC cores can be lower than 1.0 as the diameter is out of the range of Rayleigh–Debye–Gans theory, and that BC with clear shell can possibly have AAE higher than 1.0 (Bond et al., 2013;Lack and Cappa, 2010;Gyawali et al., 2009). It is also observed at the SORPES station that

Atmos. Chem. Phys. Discuss., https://doi.org/10.5194/acp-2018-49
Manuscript under review for journal Atmos. Chem. Phys.
Discussion started: 29 January 2018

$AAE_{520\text{-}880}$, which is expected to be mainly affected by BC absorption, is not always 1.0 and exhibits clear seasonal and diurnal variations (Shen et al., 2017a). Hence, assuming AAE_{BC} of 1.0 in the estimation of BrC may induce large uncertainties or errors (comparison of calculated b_{abs_BrC} assuming AAE_{BC} = 1.0 versus the modified method will be discussed later). Therefore, it is essential to firstly evaluate the quantitative impacts of BC size and coating on AAE value and determine the proper AAE_{BC} for more accurate b_{abs_BrC} calculation.

Based on core-shell Mie-theory model, we conducted a series of calculations to discuss the variation pattern of AAE for pure BC and BC with different shell (Bohren and Huffman, 1983), in which the variations of absorption property of non-absorbing (clear) and BrC (brown) coated BC particles with core size as well as coating thickness were computed. We used Christian Mätzler's code (Christian Mätzler, 2002) for Mie calculations of spherical particles at different wavelengths. Detailed calculation is described in the Supplementary Information (SI).

Mie-theory simulations were conducted firstly for single particles. Here particle core diameter (D_c) is defined as the diameter of the core alone and the shell diameter (D_p) refers to the total particle diameter. Coating thickness was represented using V_p/V_c, where V_p and V_c stands for the volume of the particle and core, respectively. D_c increases from 1 to 200 nm with 1 nm interval and V_p/V_c was set to be 1.0~8.0 with 100 bins. Here the upper limit of V_p/V_c 8.0 is based on the coating condition of carbonaceous aerosols at the SORPES station (derived from the measurement of OC and EC).

For single BC cores, the variations of $AAE_{370\text{-}520}$ and $AAE_{520\text{-}880}$ with D_c and V_p/V_c of clear and brown shell are shown in Figure 1. It shows that $AAE_{370\text{-}520}$ and $AAE_{520\text{-}880}$ of clear coated BC are mainly varying within a certain range of 0.5~1.5 (Figure 1). While due to the strong wavelength dependency, $AAE_{370\text{-}520}$ of brown coated BC is significantly higher than $AAE_{520\text{-}880}$. Also noticed in Fig. 1 is that for V_p/V_c =1.0, which means pure BC core (also shown in Fig. S2a), both $AAE_{370\text{-}520}$ and $AAE_{520\text{-}880}$ change non-monotonously with D_c. Optical interpretation based on MAE and AAE further shows that for pure BC particles, AAE firstly increases with D_c, and starts decreasing as D_c grows. For AAE

Atmos. Chem. Phys. Discuss., https://doi.org/10.5194/acp-2018-49
Manuscript under review for journal Atmos. Chem. Phys.
Discussion started: 29 January 2018

between longer wavelengths, the maximum AAE occurs with larger D_c. Detailed theoretical explanation of AAE variation for pure BC is illustrated in the SI. The same changing pattern of $AAE_{370\text{-}520}$ and $AAE_{520\text{-}880}$ (increase at first and then drop as D_c keep increasing) is also found for BC with coating, as Fig. 1 (a-b) shows. Above results clearly suggest that AAE of both pure BC particles or clear coated BC can be affected by their sizes and it is not a monotonous change, which means in real situation where BC sizes keep changing, AAE_{BC} can change as well and therefore assuming AAE as a constant is not adaptable.

Then, the MAE and AAE were calculated for a plume with a given lognormal number size distribution of BC particles (the size distribution was assumed based on previous researches with similar aerosol property at the SORPES station, shown in Fig. S4) with clear or brown coating. Figure 2 illustrates the variation of $AAE_{370\text{-}520}$ and $AAE_{520\text{-}880}$ versus V_p/V_c. Firstly, it is noticed that for a group of clear coated BC particles (dash lines), $AAE_{520\text{-}880}$ and $AAE_{370\text{-}520}$ are not always 1.0 due to the existence of larger BC cores and different coating thicknesses, instead, they both show an 'increase-steady' trend varying within the range of 1.1~1.3 and 0.9~1.0, respectively, as V_p/V_c grows. Moreover, $AAE_{370\text{-}520}$ of clear coated BC particles does not equal to $AAE_{520\text{-}880}$ and it is always lower than $AAE_{520\text{-}880}$ with different coating thicknesses. While for brown coated BC, $AAE_{370\text{-}520}$ become obviously higher than $AAE_{520\text{-}880nm}$ when coating thickness increases and $AAE_{370\text{-}520}$ value reaches to 2.2 when V_p/V_c is about 8.0 (D_p/D_c equals to 2.0), which is almost twice of $AAE_{520\text{-}880}$. Also, it can be found in Fig. 2 that for clear coated BC, $AAE_{370\text{-}520}$ and $AAE_{520\text{-}880}$ exhibit a similar variation trend, and with coating thickness varying, the ratio of $AAE_{370\text{-}520}$ /$AAE_{520\text{-}880}$ does not change much. Therefore, a correction factor $R_{s\text{-}l}$ is defined to calculate $AAE_{BC370\text{-}520}$:

$$R_{s\text{-}l} = AAE_{clear,370\text{-}520nm} / AAE_{clear,520\text{-}880nm} \quad Eq.\ 4$$

$$AAE_{BC370\text{-}520} = AAE_{520\text{-}880} \times R_{s\text{-}l} \quad Eq.\ 5$$

where $AAE_{clear,370\text{-}520nm}$ and $AAE_{clear,520\text{-}880nm}$ represent the AAE at corresponding wavelengths of clear coated BC. In this study, $R_{s\text{-}l}$ was set to be 0.85 which is the mean value from Mie-theory simulation.

Atmos. Chem. Phys. Discuss., https://doi.org/10.5194/acp-2018-49
Manuscript under review for journal Atmos. Chem. Phys.
Discussion started: 29 January 2018

When calculating $b_{abs\_BC\_370}$ according to *Eq. 1*, $AAE_{520\text{-}880}$ from aethalometer data was used which is approximately $AAE_{BC520\text{-}880}$ for stations where main absorber is BC (Lack and Langridge, 2013). $AAE_{BC370\text{-}520}$ was calculated from *Eq. 4* and *Eq. 5* instead of using the constant 1.0 based on above results. Then, b_{abs_BrC} can be derived from *Eq. 2*.

Figure 3 shows the comparison between derived b_{abs_BrC} using conventional method (assume AAE_{BC}=1) and modified one. It can be clearly observed that calculating b_{abs_BrC} assuming AAE_{BC}=1 leads to a large amount of negative values, especially in less polluted periods (also shown in the time series figure in Fig. S5). While by using modified method, long-term b_{abs_BrC} can be obtained without many invalid data and the variations of b_{abs_BrC} is corresponding to $PM_{2.5}$ level.

Since distinct difference of AAE variation versus V_p/V_c for clear and brown coated BC was found from Mie-simulation (shown in Fig. 2), $AAE_{370\text{-}520}$ and $AAE_{520\text{-}880}$ from field observation were calculated to see their variations with V_{OM}/V_{EC} in order to find out whether OC contains light absorbing contents. The results are illustrated in Fig. 4. Compared to $AAE_{520\text{-}880}$, field observed $AAE_{370\text{-}520}$ exhibits a clearer increase from 0.92 to 1.20 in average with V_{OM}/V_{EC}, and it can even reach to higher than 1.6 for V_{OM}/V_{EC} gets high. While the variation range of measured $AAE_{520\text{-}880}$ versus V_{OM}/V_{EC} is smaller (from 0.85 to 0.95) than that of $AAE_{370\text{-}520}$. Figure 4b also reveals that $AAE_{370\text{-}520}$ (blue solid circle) is higher than $AAE_{520\text{-}880}$ (red circle). Overall, the profiles of measured $AAE_{370\text{-}520}$ and $AAE_{520\text{-}880}$ are similar to the simulated brown shell lines in Fig. 2. Moreover, $AAE_{370\text{-}520}$ shows a continuous increase versus V_{OM}/V_{EC}, which is also closer to the brown shell situation in Fig. 2. Compared to that, the simulated $AAE_{370\text{-}520}$ of clear coating starts dropping after V_p/V_c exceeds 4.0. These findings indicate that the existence of BrC is highly possible contributing to the light absorption at this site.

The measured and simulated MAE were then compared to further explore the light absorption characteristics at the SORPES station and the result is shown in Fig. 5. As mentioned in Section 2.4, simulated MAE was computed for a group of BC particles with a given lognormal number size

Atmos. Chem. Phys. Discuss., https://doi.org/10.5194/acp-2018-49
Manuscript under review for journal Atmos. Chem. Phys.
Discussion started: 29 January 2018

distribution. For D_p/D_c =1.5, simulated $MAE_{370\ nm}$ of brown and clear shell are 10.4 $m^2\ g^{-1}$ and 8.6 $m^2\ g^{-1}$, respectively and $MAE_{880\ nm}$ are 3.2 $m^2\ g^{-1}$ and 3.1 $m^2\ g^{-1}$. When D_p/D_c =2.0, simulated $MAE_{370\ nm}$ of brown and clear shell exhibit large difference, which are 17.2 $m^2\ g^{-1}$ and 10.2 $m^2\ g^{-1}$, respectively, while $MAE_{880\ nm}$ values of brown and clear shell are similar. Measured MAE at each wavelength was calculated as b_{abs}/EC and then seasonal mean MAE in winter and summer are plotted also in Fig. 5. The seasonal mean $MAE_{370\ nm}$ in winter and summer are 11.4 $m^2\ g^{-1}$ and 8.6 $m^2\ g^{-1}$, respectively, and the values are 4.2 $m^2\ g^{-1}$ and 3.8 $m^2\ g^{-1}$ for $MAE_{880\ nm}$ (Table S1). Since the highest and the lowest measured MAE occurs in winter and summer, respectively, the shaded area therefore can represent the variation range of observed MAE. Figure 5 is plotted in logarithm x-y axis. Therefore, according to the definition of AAE, the slope of lines between two wavelengths in this figure represents the corresponding AAE. It can be found that MAE from field observation exhibits a similar pattern with simulated brown coating MAE lines, which shows an obvious higher slope starting from 520 nm to 370 nm. Above pattern indicates the presence of brown coated BC apart from clear coated ones at this site.

4 Long-term characteristics of BrC light absorption at the SORPES station

Based on above results, b_{abs_BrC} was determined with one-hour time interval following *Eq. 1* and *Eq. 2*. P_{BrC}, defined as the contribution of light absorption by BrC at 370 nm ($P_{BrC} = \frac{b_{abs\_BrC}}{b_{abs\_370}}$), was also calculated using the measurement data. Statistical overview is summarized in Table 1. Seasonal cycles of b_{abs_BrC} and P_{BrC} are shown in Fig. 6, together with, K^+, $K^+/PM_{2.5}$, $PM_{2.5}$ and AAE at different wavelength ranges. Firstly, it can be found that b_{abs_BrC} exhibits a distinct two-peak seasonal pattern where the peak value occurs in June and December, with mean b_{abs_BrC} of 4.2 Mm^{-1} and 11.5 Mm^{-1}, respectively (Fig. 6a). It is also observed that b_{abs_BrC} during winter, especially December, is much higher than that in other three seasons (two to three times higher). P_{BrC} also presents a two-peak seasonal trend with the high P_{BrC} months of May-June and December. The mean P_{BrC} in winter and summer are 13.8% and 9.5%, respectively, which is lower than that in Xi'an but higher than the PRD region (Shen et al., 2017b;Yuan et al., 2016). The highest P_{BrC} can reach to 28% in June and December,

Atmos. Chem. Phys. Discuss., https://doi.org/10.5194/acp-2018-49
Manuscript under review for journal Atmos. Chem. Phys.
Discussion started: 29 January 2018

which certainly cannot be ignored in light absorption estimation in the YRD region. Notably, P_{BrC} has a similar seasonal variation pattern with K^+, except in February when intensive fireworks during the Chinese New Year can lead to significantly high values of K^+ concentrations. Moreover, both $AAE_{370-520}$ and $AAE_{520-880}$ show distinct seasonal variations, but $AAE_{370-520}$ has much wider range of changing from 0.6 to 1.9, than that of $AAE_{520-880}$ (from 0.6 to 1.2). Also noticed is that the variation pattern of AAE is similar with K^+. Since K^+ is mainly emitted from primary combustion processes related to biomass, the simultaneous variation of P_{BrC} and AAE with K^+ suggests that primary emissions are likely to make considerable contribution to BrC in this area for the most of time. Comparing the seasonal pattern of P_{BrC} with $PM_{2.5}$ and $K^+/PM_{2.5}$ (Fig. 6b), it can be found that monthly variation of P_{BrC} is similar to $K^+/PM_{2.5}$ but with a clear exception in December, when P_{BrC} is in the highest level but not for $K^+/PM_{2.5}$. Such kind of difference indicates that there are other emissions besides biomass burning that may lead to the high BrC absorption in December.

Due to the distinct seasonal trend of b_{abs_BrC} observed at the SORPES station and its considerable contribution to the light absorption, it is essential to recognize the potential source areas and types of BrC in the YRD region. The diurnal variation of b_{abs_BrC} was compared to b_{abs_BC} in each season, shown in Fig. 7. Hourly mean values of b_{abs_BrC} and b_{abs_BC} are plotted. The reason to compare b_{abs_BrC} with b_{abs_BC} is that BC is one of the major light absorbers in the atmosphere and it is mostly from primary emission sources. Some kinds of the emission sources (e.g. traffic emissions) can be diagnosed by the diurnal variations. Overall, b_{abs_BrC} shows quite similar diurnal pattern with b_{abs_BC} in four seasons, which was high during night and start decreasing after sunrise. This indicates that BrC at the site is also dominated by primary emissions. The lowest values occurred in the afternoon due to the development of Planetary Boundary Layer (PBL). It is observed that b_{abs_BC} exhibits clear morning peaks in all four seasons, suggesting that traffic exhaust is likely to be a considerable emission source of BC at this site. Compared to that, the morning peaks of b_{abs_BrC} can be also observed in summer and autumn, but less obvious than that of BC, while in winter and spring the morning peaks are not noticeable. Such difference reveals that during winter and spring, traffic emission is not the main contributor to local BrC.

Atmos. Chem. Phys. Discuss., https://doi.org/10.5194/acp-2018-49
Manuscript under review for journal Atmos. Chem. Phys.
Discussion started: 29 January 2018

In order to investigate the potential source region of BrC at the SORPES station, Lagrangian particle dispersion modeling (LPDM) were conducted following the method developed by Ding et al. (2013b) by using the Hybrid Single-Particle Lagrangian Integrated Trajectory (HYSPLIT) model (R Draxler and Hess, 1998;Stein et al., 2015). The meteorological data used in this model was GDAS (Global Data Assimilation System) data with a spatial resolution of 0.05° in both latitude and longitude. In each simulation, 3000 particles were released at an altitude of 100 m above the ground level (Wang et al., 2017a) and backwardly run for a 3-day period, and then the retroplume, i.e. footprint of surface 100 m, were obtained following the method of Ding et al. (2013b).

As shown in Fig. 6a, the two distinct peaks of b_{abs_BrC} is in June and December, respectively. It is then necessary to explore the possible emission sources in these two months. As mentioned before, since BrC is an operational definition, it is difficult to perform source apportionment for BrC. The feasible way to determine its sources is to compare the relationships between BrC and certain species that are possibly from the same emission sources. Since the emission of BrC is usually related to biomass burning (Laskin et al., 2015;Saleh et al., 2014), maps of fire counts in June and December of 2014 are presented in Fig. 8, together with monthly averaged 3-day backward retroplume in order to firstly diagnose whether the majority of air plumes pass through open burning areas in these two months. Then, correlations between b_{abs_BrC} and K^+ in June and December were compared since K^+ is normally considered as a tracer of primary emission from BB (Ding et al., 2013a). The results are shown in Fig. 8 and Fig. 9.

Figure 8a shows intensive open burning, detected in June from the northwest of the site, but in this month air plumes are mainly transported from the eastern area of Nanjing where fire spots can also be found but less concentrated than northwestern regions. Contrarily, very few fire counts can be detected in December, suggesting the much less open burning events in this month. Therefore, the high level of

Atmos. Chem. Phys. Discuss., https://doi.org/10.5194/acp-2018-49
Manuscript under review for journal Atmos. Chem. Phys.
Discussion started: 29 January 2018

b_{abs_BrC} in December is not likely to be from BB emissions. Map of retroplume reveals that air masses are mainly from the north area in December. Then, correlations between daily average b_{abs_BrC} and K^+ mass concentration in June and December is compared as Fig. 9a shows. It can be observed that the correlations between b_{abs_BrC} and K^+ in these two months exhibit a clearly different pattern. The slope of fitted b_{abs_BrC} and K^+ in June is 3.35 and the correlation coefficient R^2 is 0.93. Knowing the strong correlation between b_{abs_BrC} and K^+ in June, combined with the observed intense fire counts in this month, it can be presumed that primary BB emission can be a major contributor of BrC during June. As for December, b_{abs_BrC} and K^+ presents a much lower correlation coefficient (R^2 = 0.25) and the slope is 7.79, which is approximately twice as that in June. The distribution of b_{abs_BrC}/K^+ in these two seasons are shown in Fig. 9b. The result displays that b_{abs_BrC}/K^+ of June and December have a significant difference (through t-test, $P < 0.05$), proving that the dominant emission source of BrC in December is not biomass burning (significant difference test of b_{abs_BrC}/K^+ is also done for May and June, which are the main BB seasons for comparison, and the result shows that there is no significant difference in these two months, Fig. S6).

Above analyses have demonstrated that BrC is not mainly from biomass burning and vehicle exhausts in December. Since large number of BrC is from combustion processes, and it is noticed from emission inventory that Cl^- and OC both take up a higher percentage from combustion emission compared to other source sectors (Fu et al., 2013). Therefore, to further explore the potential sources of such high BrC in winter season, the occurrence frequencies of Cl^-/EC and OC/EC in June and December compared to the data in the whole year are calculated and illustrated in Fig. 10. The ratio of Cl^-/EC is calculated to firstly eliminate the impact of PBL in different seasons and can be considered as the indicator of coal combustion emission in non-BB season. As presented in Fig. 10a, Cl^-/EC during the whole year is mainly distributed in the range of 0~0.5 and this ratio in June is comparable to the yearly overall level. While in December, the distribution of Cl^-/EC is apparently higher, with the value varies at around 0.5~1.5, indicating the possibility of the impact from coal combustion in this month. It is reported that although industrial coal consumption has been reduced in recent years in China, the

Atmos. Chem. Phys. Discuss., https://doi.org/10.5194/acp-2018-49
Manuscript under review for journal Atmos. Chem. Phys.
Discussion started: 29 January 2018

contribution of residential coal combustion to primary $PM_{2.5}$ emission is in a high percentage and the number keeps increasing (Li et al., 2016;Zhao et al., 2013). Moreover, the emission inventory in the YRD region reveals that residential combustion is much higher in winter than in other seasons due to the large number of domestic heating, while power plant and industrial emission level are basically stable in all seasons without apparent difference in winter (Fu et al., 2013;Wang et al., 2011). Therefore, after precluding the possibility of BB effects on BrC in this month, the obvious high Cl^-/EC in winter is more likely related to residential coal combustion. As for OC/EC, the distribution patterns in June and December are quite different compared to all-year situation, which are lower and higher than yearly distribution, respectively, with the occurrence frequencies of OC/EC peaking at 1.6 and 2.4, while the fire count numbers in December is quite small. This phenomenon indicates that BB is not the major source of BrC in December. Overall, residential coal burning is the most possible emission source of BrC in winter month in YRD region.

5 Summary

In this study, light absorption of BrC was quantified using the optical method based on the definition of BrC. Mie-theory simulation and observational results were combined to improve this method by calculating AAE_{BC} at each time point instead of assuming a constant. Long-term variation of b_{abs_BrC} and P_{BrC} were then derived. Apparent light absorption contributed by BrC is discovered in YRD region. b_{abs_BrC} and P_{BrC} both exhibit clear seasonal cycles with two peaks in May to June and December. The light absorption contribution of BrC at 370 nm ranges from 6% to 18% (for 10th and 90th percentiles), and can reach to 28% in BB-dominant season and winter season, which is lower than Xi'an but higher than PRD region. Comparison between b_{abs_BrC} and b_{abs_BC} suggests that vehicle emission makes negligible impact on regional BrC level during winter and spring. Source analysis was performed based on temporal variations of BrC and the comparison of possible co-emitted pollutants or related parameters including K^+, Cl^-, BC and OC. Lagrangian particle dispersion modeling (LPDM) and MODIS fire data were also used to support analysis. The month of June and December with the peak level of b_{abs_BrC} are chosen to analyze the potential emission sources of BrC and it is found that the

high contributions of BrC in these two months are dominated by different emission sources. In June, intensive primary BB emission is the dominant source of BrC, making b_{abs_BrC} appears short-time high values raising its average level in this month. While in December, BB is not the major source of BrC and the high level of BrC is contributed by residential sources, highly possible to be dominated by residential coal combustion.

Overall, this work explores an improved optical method to quantify b_{abs_BrC} from long-term observation. Compared to the conventional one, which have high uncertainty due to the assumption of constant AAE_{BC} regardless of its variation with particle size, wavelength and time, and can only be used when BrC contribution is high, this improved method is applicable for those sites where BrC proportion is lower and make it available for long-term analysis. This study also highlights the considerable contribution of BrC to light absorption at near UV range in the YRD region. Moreover, different emission sources of BrC is found in different seasons, providing a clearer reference for mitigation measures as well as regional control policies in eastern China.

Acknowledgements:

This work was supported by Ministry of Science and Technology of the People's Republic of China 20 (2016YFC0200500), the National Natural Science Foundation of China (91544231, 41725020, and 41422504), and the Public Welfare Projects for Environmental Protection (201509004).

References

Aiken, A. C., DeCarlo, P. F., Kroll, J. H., Worsnop, D. R., Huffman, J. A., Docherty, K. S., Ulbrich, I. M., Mohr, C., Kimmel, J. R., Sueper, D., Sun, Y., Zhang, Q., Trimborn, A., Northway, M., Ziemann, P. J., Canagaratna, M. R., Onasch, T. B., Alfarra, M. R., Prevot, A. S. H., Dommen, J., Duplissy, J., Metzger, A., Baltensperger, U., and Jimenez, J. L.: O/C and OM/OC Ratios of Primary, Secondary, and Ambient Organic Aerosols with High-Resolution Time-of-Flight Aerosol Mass Spectrometry, Environ. Sci. Technol., 42, 4478-4485, 10.1021/es703009q, 2008.

Andreae, M. O., and Gelencsér, A.: Black carbon or brown carbon? The nature of light-absorbing carbonaceous aerosols, Atmos. Chem. Phys. , 6, 3131-3148, 10.5194/acp-6-3131-2006, 2006.

Bahadur, R., Praveen, P. S., Xu, Y. Y., and Ramanathan, V.: Solar absorption by elemental and brown carbon determined from spectral observations, PNAS 109, 17366-17371, 10.1073/pnas.1205910109, 2012.

Bond, T. C., Doherty, S. J., Fahey, D. W., Forster, P. M., Berntsen, T., DeAngelo, B. J., Flanner, M. G., Ghan, S., Kärcher, B., Koch, D., Kinne, S., Kondo, Y., Quinn, P. K., Sarofim, M. C., Schultz, M. G., Schulz, M., Venkataraman, C., Zhang, H., Zhang, S., Bellouin, N., Guttikunda, S. K., Hopke, P. K., Jacobson, M. Z., Kaiser, J. W., Klimont, Z., Lohmann, U., Schwarz, J. P., Shindell, D., Storelvmo, T., Warren, S. G., and Zender, C. S.: Bounding the role of black carbon in the climate system: A scientific assessment, J. Geophys. Res.-Atmos. , 118, 5380-5552, 10.1002/jgrd.50171, 2013.

Cao, G., Zhang, X., and Zheng, F.: Inventory of black carbon and organic carbon emissions from China, Atmos. Environ. , 40, 6516-6527, https://doi.org/10.1016/j.atmosenv.2006.05.070, 2006.

Cao, J.-J., Zhu, C.-S., Chow, J. C., Watson, J. G., Han, Y.-M., Wang, G.-h., Shen, Z.-x., and An, Z.-S.: Black carbon relationships with emissions and meteorology in Xi'an, China, Atmos. Res. , 94, 194-202, https://doi.org/10.1016/j.atmosres.2009.05.009, 2009.

Cavalli, F., Facchini, M. C., Decesari, S., Mircea, M., Emblico, L., Fuzzi, S., Ceburnis, D., Yoon, Y. J., O'Dowd, C. D., Putaud, J. P., and Dell'Acqua, A.: Advances in characterization of size-resolved organic matter in marine aerosol over the North Atlantic, J. Geophys. Res.-Atmos. , 109, n/a-n/a, 10.1029/2004JD005137, 2004.

Chen, Y., and Bond, T. C.: Light absorption by organic carbon from wood combustion, Atmos. Chem. Phys. , 10, 1773-1787, 2010.

Collaud Coen, M., Weingartner, E., Apituley, A., Ceburnis, D., Fierz-Schmidhauser, R., Flentje, H., Henzing, J., Jennings, S. G., Moerman, M., and Petzold, A.: Minimizing light absorption measurement artifacts of the Aethalometer: evaluation of five correction algorithms, Atmos. Meas. Tech., 3, 457-474, 2010.

Dalzell, W. H., and Sarofim, A. F.: Optical Constants of Soot and Their Application to Heat-Flux Calculations, J. Heat Transfer 91, 100-104, 10.1115/1.3580063, 1969.

Ding, A., Fu, C., Yang, X., Sun, J., Petäjä, T., Kerminen, V.-M., Wang, T., Xie, Y., Herrmann, E., and Zheng, L.: Intense atmospheric pollution modifies weather: a case of mixed biomass burning with fossil fuel combustion pollution in eastern China, Atmos. Chem. Phys. , 13, 10545-10554, 2013a.

Ding, A., Wang, T., and Fu, C.: Transport characteristics and origins of carbon monoxide and ozone in Hong Kong, South China, J. Geophys. Res.-Atmos. , 118, 9475-9488, 2013b.

Ding, A., Nie, W., Huang, X., Chi, X., Sun, J., Kerminen, V.-M., Xu, Z., Guo, W., Petäjä, T., Yang, X.,

Kulmala, M., and Fu, C.: Long-term observation of air pollution-weather/climate interactions at the SORPES station: a review and outlook, Frontiers of Environmental Science & Engineering, 10, 15-, 10.1007/s11783-016-0877-3, 2016a.

Ding, A. J., Fu, C. B., Yang, X. Q., Sun, J. N., Zheng, L. F., Xie, Y. N., Herrmann, E., Nie, W., Petäjä, T., Kerminen, V. M., and Kulmala, M.: Ozone and fine particle in the western Yangtze River Delta: an overview of 1 yr data at the SORPES station, Atmos. Chem. Phys. , 13, 5813-5830, 10.5194/acp-13-5813-2013, 2013c.

Ding, A. J., Huang, X., Nie, W., Sun, J., Kerminen, V. M., Petaja, T., Su, H. L., Cheng, Y. F., Yang, X. Q., and Wang, M.: Black carbon enhances haze pollution in megacities in China, Geophys. Res. Lett. , 2016b.

Dockery, D. W., Pope, C. A., Xu, X., Spengler, J. D., Ware, J. H., Fay, M. E., Ferris, B. G., and Speizer, F. E.: An Association between Air Pollution and Mortality in Six U.S. Cities, N. Engl. J. Med., 329, 1753-1759, doi:10.1056/NEJM199312093292401, 1993.

Feng, Y., Ramanathan, V., and Kotamarthi, V. R.: Brown carbon: a significant atmospheric absorber of solar radiation?, Atmos. Chem. Phys. , 13, 8607-8621, 10.5194/acp-13-8607-2013, 2013.

Fu, X., Wang, S., Zhao, B., Xing, J., Cheng, Z., Liu, H., and Hao, J.: Emission inventory of primary pollutants and chemical speciation in 2010 for the Yangtze River Delta region, China, Atmos. Environ. , 70, 39-50, https://doi.org/10.1016/j.atmosenv.2012.12.034, 2013.

Gyawali, M., Arnott, W. P., Lewis, K., and Moosmüller, H.: In situ aerosol optics in Reno, NV, USA during and after the summer 2008 California wildfires and the influence of absorbing and non-absorbing organic coatings on spectral light absorption, Atmos. Chem. Phys. , 9, 8007-8015, 10.5194/acp-9-8007-2009, 2009.

Hansen, A., and Schnell, R.: The aethalometer, Magee Scientific Company, Berkeley, California, USA, 1-209, 2005.

Huang, R.-J., Zhang, Y., Bozzetti, C., Ho, K.-F., Cao, J.-J., Han, Y., Daellenbach, K. R., Slowik, J. G., Platt, S. M., Canonaco, F., Zotter, P., Wolf, R., Pieber, S. M., Bruns, E. A., Crippa, M., Ciarelli, G., Piazzalunga, A., Schwikowski, M., Abbaszade, G., Schnelle-Kreis, J., Zimmermann, R., An, Z., Szidat, S., Baltensperger, U., Haddad, I. E., and Prévôt, A. S. H.: High secondary aerosol contribution to particulate pollution during haze events in China, Nature, 514, 218, 10.1038/nature13774
https://www.nature.com/articles/nature13774#supplementary-information, 2014.

IPCC: Climate Change 2013: The Physical Science Basis. Contribution of Working Group I to the Fifth Assessment Report of the Intergovernmental Panel on Climate Change, Cambridge University Press, Cambridge, United Kingdom and New York, NY, USA, 1535 pp., 2013.

Lack, D., and Cappa, C.: Impact of brown and clear carbon on light absorption enhancement, single scatter albedo and absorption wavelength dependence of black carbon, Atmos. Chem. Phys. , 10, 4207-4220, 2010.

Lack, D. A., Langridge, J. M., Bahreini, R., Cappa, C. D., Middlebrook, A. M., and Schwarz, J. P.: Brown carbon and internal mixing in biomass burning particles, Proceedings of the National Academy of Sciences of the United States of America, 109, 14802-14807, 10.1073/pnas.1206575109, 2012.

Lack, D. A., and Langridge, J. M.: On the attribution of black and brown carbon light absorption using

the Ångström exponent, Atmos. Chem. Phys. , 13, 10535-10543, 2013.

Laskin, A., Laskin, J., and Nizkorodov, S. A.: Chemistry of atmospheric brown carbon, Chem. Rev., 115, 4335-4382, 10.1021/cr5006167, 2015.

Li, Q., Li, X., Jiang, J., Duan, L., Ge, S., Zhang, Q., Deng, J., Wang, S., and Hao, J.: Semi-coke briquettes: towards reducing emissions of primary PM(2.5), particulate carbon, and carbon monoxide from household coal combustion in China, Sci. Rep., 6, 19306, 10.1038/srep19306, 2016.

Moosmüller, H., Chakrabarty, R. K., Ehlers, K. M., and Arnott, W. P.: Absorption Ångström coefficient, brown carbon, and aerosols: basic concepts, bulk matter, and spherical particles, Atmos. Chem. Phys. , 11, 1217-1225, 10.5194/acp-11-1217-2011, 2011.

Olson, M. R., Victoria Garcia, M., Robinson, M. A., Van Rooy, P., Dietenberger, M. A., Bergin, M., and Schauer, J. J.: Investigation of black and brown carbon multiple-wavelength-dependent light absorption from biomass and fossil fuel combustion source emissions, J. Geophys. Res.-Atmos. , 120, 6682-6697, 10.1002/2014JD022970, 2015.

Pöschl, U.: Aerosol particle analysis: challenges and progress, Anal. Bioanal.Chem., 375, 30-32, 10.1007/s00216-002-1611-5, 2003.

Pitchford, M., Malm, W., Schichtel, B., Kumar, N., Lowenthal, D., and Hand, J.: Revised Algorithm for Estimating Light Extinction from IMPROVE Particle Speciation Data, J. Air Waste manage., 57, 1326-1336, 10.3155/1047-3289.57.11.1326, 2007.

R Draxler, R., and Hess, G.: An overview of the HYSPLIT_4 modeling system for trajectories, dispersion, and deposition, 295-308 pp., 1998.

Saleh, R., Robinson, E. S., Tkacik, D. S., Ahern, A. T., Liu, S., Aiken, A. C., Sullivan, R. C., Presto, A. A., Dubey, M. K., Yokelson, R. J., Donahue, N. M., and Robinson, A. L.: Brownness of organics in aerosols from biomass burning linked to their black carbon content, Nat. Geosci. , 7, 647, 10.1038/ngeo2220
https://www.nature.com/articles/ngeo2220#supplementary-information, 2014.

Shen, Y., Virkkula, A., Ding, A., Wang, J., Chi, X., Nie, W., Qi, X., Huang, X., Liu, Q., Zheng, L., Xu, Z., Petäjä, T., Aalto, P. P., Fu, C., and Kulmala, M.: Aerosol Optical Properties at SORPES in Nanjing, East China, Atmos. Chem. Phys. Discuss., 2017, 1-46, 10.5194/acp-2017-863, 2017a.

Shen, Z., Lei, Y., Zhang, L., Zhang, Q., Zeng, Y., Tao, J., Zhu, C., Cao, J., Xu, H., and Liu, S.: Methanol Extracted Brown Carbon in PM2.5 Over Xi'an, China: Seasonal Variation of Optical Properties and Sources Identification, Aerosol Sci. Eng., 1, 57-65, 10.1007/s41810-017-0007-z, 2017b.

Stein, A. F., Draxler, R. R., Rolph, G. D., Stunder, B. J. B., Cohen, M. D., and Ngan, F.: NOAA's HYSPLIT Atmospheric Transport and Dispersion Modeling System, Bull. Am. Meteorol. Soc. , 96, 2059-2077, 10.1175/bams-d-14-00110.1, 2015.

Stone, E. A., Hedman, C. J., Sheesley, R. J., Shafer, M. M., and Schauer, J. J.: Investigating the chemical nature of humic-like substances (HULIS) in North American atmospheric aerosols by liquid chromatography tandem mass spectrometry, Atmos. Environ. , 43, 4205-4213, https://doi.org/10.1016/j.atmosenv.2009.05.030, 2009.

Sun, H., Biedermann, L., and Bond, T. C.: Color of brown carbon: A model for ultraviolet and visible light absorption by organic carbon aerosol, Geophys. Res. Lett. , 34, 10.1029/2007gl029797, 2007.

Virkkula, A., Chi, X., Ding, A., Shen, Y., Nie, W., Qi, X., Zheng, L., Huang, X., Xie, Y., Wang, J.,

Petäjä, T., and Kulmala, M.: On the interpretation of the loading correction of the aethalometer, Atmos. Meas. Tech., 8, 4415-4427, 10.5194/amt-8-4415-2015, 2015.

Wang, J., Virkkula, A., Gao, Y., Lee, S., Shen, Y., Chi, X., Nie, W., Liu, Q., Xu, Z., Huang, X., Wang, T., Cui, L., and Ding, A.: Observations of aerosol optical properties at a coastal site in Hong Kong, South China, Atmos. Chem. Phys. , 17, 2653-2671, 10.5194/acp-17-2653-2017, 2017a.

Wang, J., Xing, J., Mathur, R., Pleim, J. E., Wang, S., Hogrefe, C., Gan, C.-M., Wong, D. C., and Hao, J.: Historical trends in PM2. 5-related premature mortality during 1990–2010 across the northern hemisphere, Environ. Health Perspect. , 125, 400, 2017b.

Wang, J., Zhao, B., Wang, S., Yang, F., Xing, J., Morawska, L., Ding, A., Kulmala, M., Kerminen, V.-M., Kujansuu, J., Wang, Z., Ding, D., Zhang, X., Wang, H., Tian, M., Petäjä, T., Jiang, J., and Hao, J.: Particulate matter pollution over China and the effects of control policies, Sci. Total Environ. , 584-585, 426-447, https://doi.org/10.1016/j.scitotenv.2017.01.027, 2017c.

Wang, S., Xing, J., Chatani, S., Hao, J., Klimont, Z., Cofala, J., and Amann, M.: Verification of anthropogenic emissions of China by satellite and ground observations, Atmos. Environ. , 45, 6347-6358, https://doi.org/10.1016/j.atmosenv.2011.08.054, 2011.

Yang, M., Howell, S. G., Zhuang, J., and Huebert, B. J.: Attribution of aerosol light absorption to black carbon, brown carbon, and dust in China – interpretations of atmospheric measurements during EAST-AIRE, Atmos. Chem. Phys. , 9, 2035-2050, 10.5194/acp-9-2035-2009, 2009.

Yuan, J. F., Huang, X. F., Cao, L. M., Cui, J., Zhu, Q., Huang, C. N., Lan, Z. J., and He, L. Y.: Light absorption of brown carbon aerosol in the PRD region of China, Atmos. Chem. Phys. , 16, 1433-1443, 10.5194/acp-16-1433-2016, 2016.

Zhao, B., Wang, S., Wang, J., Fu, J. S., Liu, T., Xu, J., Fu, X., and Hao, J.: Impact of national NOx and SO2 control policies on particulate matter pollution in China, Atmos. Environ. , 77, 453-463, https://doi.org/10.1016/j.atmosenv.2013.05.012, 2013.

Atmos. Chem. Phys. Discuss., https://doi.org/10.5194/acp-2018-49
Manuscript under review for journal Atmos. Chem. Phys.
Discussion started: 29 January 2018

Figure captions

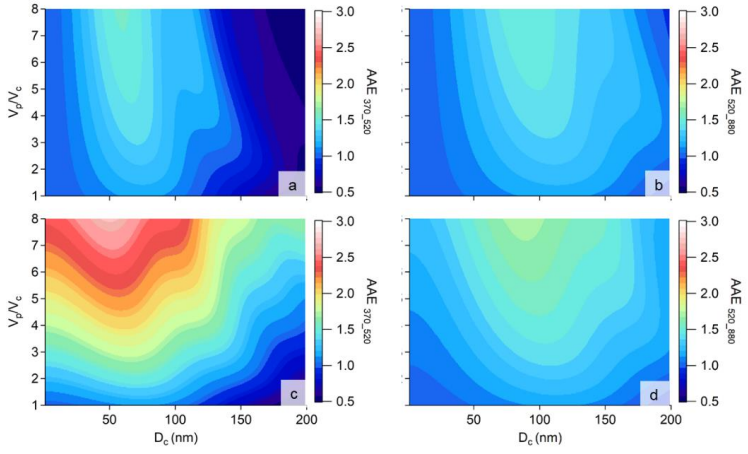

Figure 1. Variation of Absorption Ångstrom Exponents between 370 and 520 nm ($AAE_{370\text{-}520}$) and between 520 and 880 nm ($AAE_{520\text{-}880}$) along with black carbon (BC) core diameter (D_c) and the volume ration of coated particle and BC core (V_p/V_c) simulated with core-shell Mie model. (a-b) are with clear (pure scattering) shell and (c-d) are with brown shell.

Atmos. Chem. Phys. Discuss., https://doi.org/10.5194/acp-2018-49
Manuscript under review for journal Atmos. Chem. Phys.
Discussion started: 29 January 2018

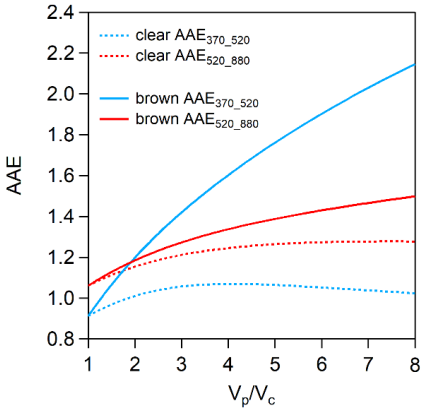

Figure 2. Variations of simulated $AAE_{370\text{-}520}$ (blue lines) and $AAE_{520\text{-}880}$ (red lines) versus V_p/V_c with a given lognormal particle number size distribution. Solid and dash lines represent BC with brown and clear shell, respectively.

Atmos. Chem. Phys. Discuss., https://doi.org/10.5194/acp-2018-49
Manuscript under review for journal Atmos. Chem. Phys.
Discussion started: 29 January 2018

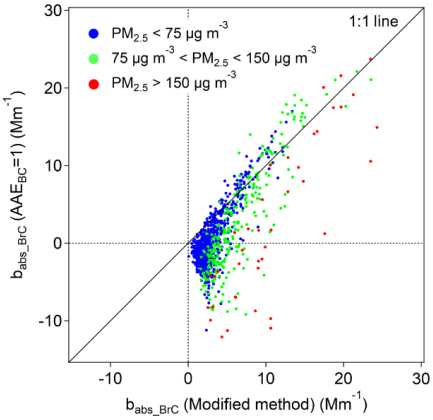

Figure 3. Comparison of calculated daily mean b_{abs_BrC} assuming AAE_{BC} = 1.0 versus using modified method. Data points are color coded by three $PM_{2.5}$ levels, which are $PM_{2.5}$ < 75 μg m^{-3} (blue), 75 μg m^{-3} < $PM_{2.5}$ < 150 μg m^{-3} (green), and $PM_{2.5}$ > 150 μg m^{-3} (red), respectively

5

Atmos. Chem. Phys. Discuss., https://doi.org/10.5194/acp-2018-49
Manuscript under review for journal Atmos. Chem. Phys.
Discussion started: 29 January 2018

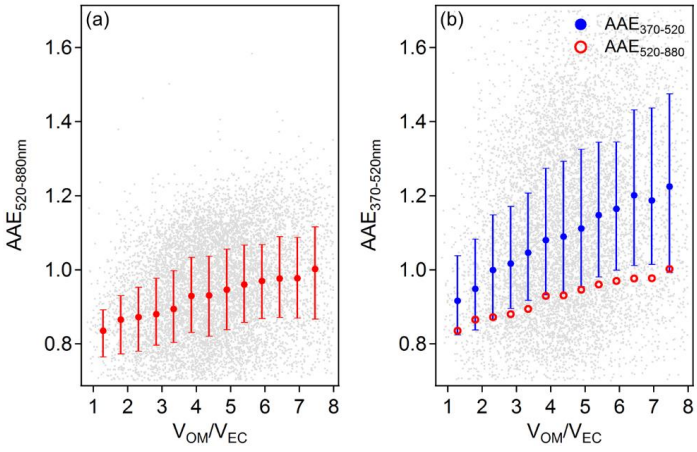

Figure 4. Relationships between AAE and V_{OM} / V_{EC}, where median values of $AAE_{520-880}$ (a) and $AAE_{370-520}$ (b) are shown as red and blue dots, respectively. Error bars represent the 25th and 75th percentile of data. The median $AAE_{520-880nm}$ is also plotted as red circle in (b) for comparison

Atmos. Chem. Phys. Discuss., https://doi.org/10.5194/acp-2018-49
Manuscript under review for journal Atmos. Chem. Phys.
Discussion started: 29 January 2018

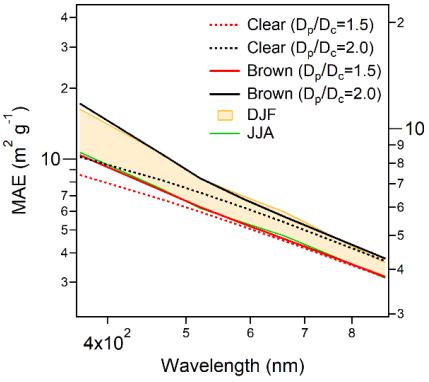

Figure 5. Observed mean MAE at SORPES station compared to simulated MAE at different wavelengths. The highest and the lowest measured value was in winter and summer, respectively, hence the shaded area represent the distribution of observed MAE. Solid and dash lines (in red and black color for different D_p/D_c) represent BC with brown and clear shell, respectively

Atmos. Chem. Phys. Discuss., https://doi.org/10.5194/acp-2018-49
Manuscript under review for journal Atmos. Chem. Phys.
Discussion started: 29 January 2018

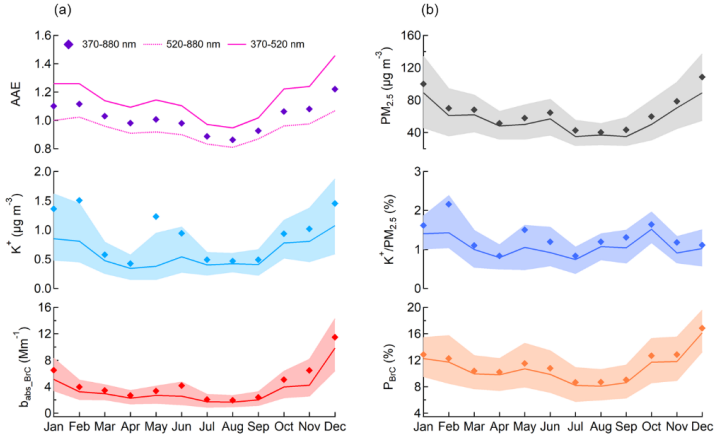

Figure 6. Seasonal cycle of (a) b_{abs_BrC}, K^+, and AAE at different wavelength ranges ($AAE_{370-520}$, $AAE_{370-880}$ and $AAE_{370-880}$, shown as solid line, dash line and diamonds, respectively) and (b) P_{BrC}, $K^+/PM_{2.5}$ and $PM_{2.5}$. For b_{abs_BrC}, K^+, P_{BrC}, $K^+/PM_{2.5}$ and $PM_{2.5}$ figures, bold solid lines represent median values, diamonds show the monthly averages and thin solid lines forming the shaded area are 25th and 75th percentiles

Atmos. Chem. Phys. Discuss., https://doi.org/10.5194/acp-2018-49
Manuscript under review for journal Atmos. Chem. Phys.
Discussion started: 29 January 2018

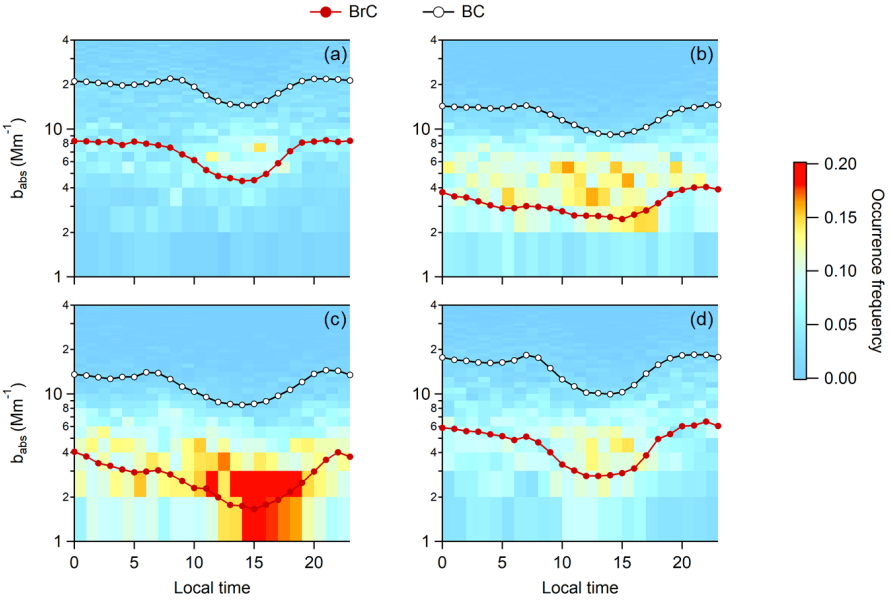

Figure 7. Diurnal variations of b_{abs_BrC} and b_{abs_BC} in four seasons (a) winter, (b) spring, (c) summer, (d) autumn. The image plot shows the occurrence frequencies of b_{abs_BrC} in each b_{abs_BrC} bins. The dark red and black circle lines represent the hourly mean b_{abs_BrC} and b_{abs_BC}, respectively.

Atmos. Chem. Phys. Discuss., https://doi.org/10.5194/acp-2018-49
Manuscript under review for journal Atmos. Chem. Phys.
Discussion started: 29 January 2018

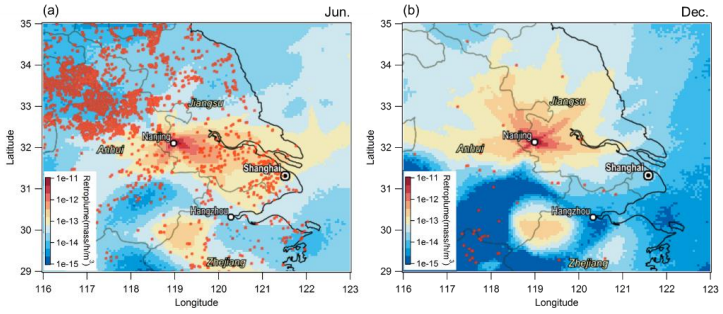

Figure 8. Map of averaged 3-day backward retroplume and the fire counts for (a) June and (b) December in 2014. Fire count data is from MODIS Collection 5 Active Fire Product provided by NASA fire mapper (https://firms.modaps.eosdis.nasa.gov/firemap/)

5

Atmos. Chem. Phys. Discuss., https://doi.org/10.5194/acp-2018-49
Manuscript under review for journal Atmos. Chem. Phys.
Discussion started: 29 January 2018

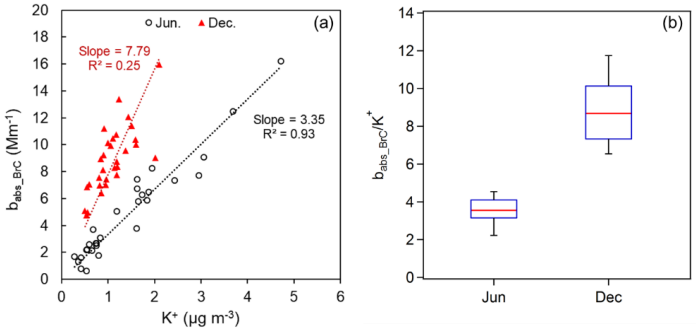

Figure 9. (a) Correlations between daily average b_{abs_BrC} and K^+ mass concentration in June (black circles) and December (red triangles); (b) Boxplot of b_{abs_BrC}/K^+ in June and December (data is from the year 2014), where red lines represent the median value, blue boxes represent 25th and 75th percentile ranges and thin bars are 5th and 95th percentiles

Atmos. Chem. Phys. Discuss., https://doi.org/10.5194/acp-2018-49
Manuscript under review for journal Atmos. Chem. Phys.
Discussion started: 29 January 2018

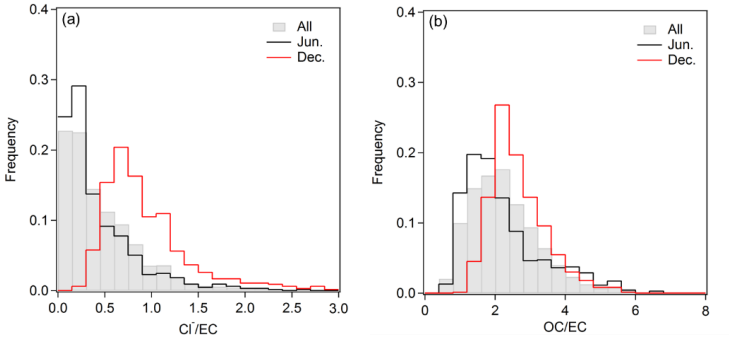

Figure 10. Occurrence frequencies of (a) Cl^-/EC and (b) OC/EC for data in June (black lines) and December (red lines) compared to all data (grey shaded bars) during 2014

5

Atmos. Chem. Phys. Discuss., https://doi.org/10.5194/acp-2018-49
Manuscript under review for journal Atmos. Chem. Phys.
Discussion started: 29 January 2018

Table 1. Statistical summary of data measured at SORPES station

	Mean	percentiles		Seasonal mean			
		1th	99th	DJF	MAM	JJA	SON
b_{abs_BrC} (Mm^{-1})	4.3	0.2	23.0	7.0	3.1	2.8	4.7
P_{BrC} (%)	11.3	2.2	27.9	13.8	10.7	9.5	11.5
b_{abs_BC} (Mm^{-1})	14.5	2.4	51.6	19.2	12.5	11.7	15.1
b_{abs_370}	35.8	5.6	136.0	51.0	29.7	26.5	37.3
b_{abs_520}	23.9	3.9	86.3	32.8	20.3	18.5	24.8
$AAE_{370\text{-}520}$	1.2	0.6	1.9	1.3	1.1	1.0	1.2
$AAE_{520\text{-}880}$	0.9	0.6	1.2	1.0	0.9	0.8	0.9
OC (μg m^{-3})	8.7	1.7	29.5	10.3	8.5	6.7	9.4
EC (μg m^{-3})	3.7	0.8	10.4	4.1	3.6	3.4	3.7
OC/EC	2.5	0.7	6.4	2.7	2.6	2.0	2.5
K^+ (μg m^{-3})	0.9	0.1	6.5	1.4	0.7	0.6	0.8
Cl^- (μg m^{-3})	2.2	0.0	12.9	4.0	2.0	0.8	1.7